Adaptive Beam Pattern Selection and Resource Allocation for NOMA-Based LEO Satellite Systems

Anyue Wang[1], Lei Lei[2], Xin Hu[3], Eva Lagunas[1], Ana I. Pérez-Neira[4], and Symeon Chatzinotas[1]

[1]Interdisciplinary Centre for Security, Reliability and Trust (SnT), University of Luxembourg, Luxembourg
[2]School of Information and Communications Engineering, Xi'an Jiaotong University, China
[3]School of Electronic Engineering, Beijing University of Posts and Telecommunications, China
[4]Centre Tecnològic de Telecomunicacions de Catalunya (CTTC/CERCA) and Universitat Politècnica de Catalunya (UPC), Spain
[1,2,3,4]*Emails: {anyue.wang; eva.lagunas; symeon.chatzinotas}@uni.lu, lei.lei@xjtu.edu.cn, huxin2016@bupt.edu.cn, ana.perez@cttc.es*

***Abstract*—The low earth orbit (LEO) satellite system is one of the promising solutions to provide broadband services to a wide-coverage area for future integrated LEO-6G networks, where users' demands vary with time and geographical locations. Conventional satellites with fixed beam pattern and footprint planning may not be capable of meeting such dynamic requests and irregular traffic distributions. As the development of flexible satellite payload with beamforming capabilities, spot beams with flexible size and shape are considered potential solutions to this issue. As an early investigation, in this paper, we consider the scenarios where satellite payloads are equipped with multiple beam patterns and study the optimal beam pattern selection. We exploit the potential synergies of joint resource optimization between adaptive beam patterns and non-orthogonal multiple access (NOMA) in a LEO satellite system, where NOMA is employed to reduce intra-beam interference and flexible beam pattern is adopted to mitigate inter-satellite interference. The formulated problem is to minimize the capacity-demand gap of terminals, which falls into mixed-integer nonconvex programming (MINCP). To tackle the discrete variables and nonconvexity, we design a joint approach to allocate power and select beam patterns. Numerical results show that the proposed scheme achieves capacity-demand gap reduction of 37.8% over conventional orthogonal multiple access (OMA) and 42.5% over the fixed-beam-pattern scheme.**

***Index Terms*—low earth orbit (LEO) satellite systems, non-orthogonal multiple access (NOMA), adaptive beam patterns**

I. Introduction

Low earth orbit (LEO) satellite systems are envisioned as one of the promising solutions for coverage extension in the upcoming beyond 5G (B5G) and 6G era [1]. To deliver exponentially growing traffic and support ubiquitous connectivity, the industry is in the process of deploying hundreds or thousands of LEO satellites in the space [2], e.g., SpaceX Starlink. However, with densely deployed LEO satellites, terminals may receive considerable interference from neighboring satellites [3]. Besides, due to the heterogeneity of traffic distribution, resource allocation in LEO satellite systems needs to be more adaptive. The mitigation of interference and provision of high-quality services are challenging, calling for the introduction of more flexibility in resource allocation [4].

In conventional satellite systems, beam patterns are fixed and the projected beam shapes (or footprints) remain constant

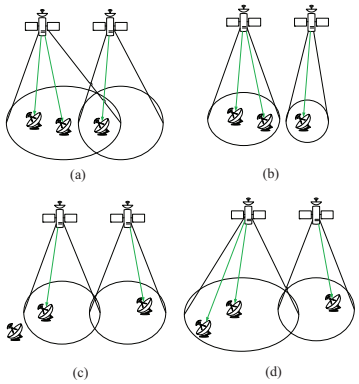

Fig. 1: Illustrative examples of adaptive beam patterns in LEO satellite systems.

[5]. When LEO satellites are densely deployed and traffic demands are irregularly distributed, this fixed beam pattern may limit the performance improvement. With the development of flexible payloads, beam shapes can be altered by changing beam patterns via beamforming networks (BFN) [5]. By adjusting beam patterns on a frame basis, satellite transmission can be more adaptive to irregular traffic distribution [6]–[8], with mitigated co-channel interference [9], and with benefits of facilitating integration with terrestrial systems [9], [10]. We provide illustrative instances of adaptive beam patterns in Fig. 1. When a terminal is located in the area covered by two adjacent satellite beams, e.g., in Fig. 1(a), the terminal may suffer from strong inter-satellite interference. To reduce the interference, both satellites could select patterns with smaller but more concentrated beams to cover the associated terminals, as depicted in Fig. 1(b). Another typical example is to change patterns with larger beams to cover terminals beyond the beam edge but with high demand, e.g., from Fig. 1(c) to Fig. 1(d).

Considering the advantages in traffic adaptation and interference mitigation, adaptive beam pattern has received significant attention. The authors in [6] jointly optimized beamwidth and transmit power to adapt to varying traffic. In [7], more factors affecting the beam shape, e.g., beam center and rotation angle, were taken into account and the footprint planning was designed to match irregular traffic distribution. In both works, the expressions of transmit antenna gain w.r.t. configuration parameters (e.g., beamwidth, beam center, rotation angle) were

GLOBECOM 2022 - 2022 IEEE Global Communications Conference | 978-1-6654-3540-6/22/$31.00 ©2022 IEEE | DOI: 10.1109/GLOBECOM48099.2022.10000986

derived. But the relationship between transmit antenna gain and configuration parameters is complex in general. Directly optimizing footprints is difficult in practical implementation [5]. Alternatively, multiple candidate beam patterns can be designed in advance for various possible scenarios and a suitable beam pattern can be selected depending on traffic distribution and interference. Beam pattern selection can be applied to both regular and irregular footprints and candidate patterns can be easily updated when necessary. In [8], the authors optimized beam pattern selection to meet irregular traffic distribution and discussed its practical implementation. The above works focused on optimizing rate matching to traffic distribution over an area instead of traffic demands of specific terminals. In this paper, we study beam pattern selection to alleviate capacaity-demand mismatch of terminals and investigate the implicit coupling between beam pattern selection and resource allocation for multiple terminals in each beam.

To facilitate the accommodation of multiple terminals in each beam, non-orthogonal multiple access (NOMA) is applied. By superposition coding and successive interference cancellation (SIC), spectral efficiency can be enhanced compared to orthogonal multiple access (OMA) [11]. NOMA has proven its advantages in LEO satellite systems, e.g., supporting massive connectivity [12] and assisting file delivery [13]. In this paper, we study resource allocation in LEO satellite systems where NOMA is applied in each satellite beam to reduce intra-beam interference whereas adaptive beam patterns are adopted to mitigate inter-satellite interference.

As an early-stage study, it is necessary to outline the optimal strategies of beam pattern selection according to heterogeneous traffic requests and characterize the mutual impacts between NOMA and adaptive beam patterns. Motivated by this, in this paper, we investigate the potential synergy of NOMA and adaptive beam patterns in LEO satellite systems. We formulate a resource allocation problem to jointly optimize power allocation and beam pattern selection, which is mixed-integer nonconvex programming (MINCP). Considering the difficulty of solving the MINCP problem, we convert the nonconvexity and binary variables into a solvable way and design a scheme to jointly optimize power and beam patterns. Numerical results verify the advantages of the joint optimization over conventional schemes, e.g., OMA and fixed beam pattern.

II. System Model and Problem Formulation

A. System Model

We consider downlink transmission in a LEO satellite system, as depicted in Fig. 2. S satellites fly over the area of interest, where the coverages may overlap partially with neighboring satellite beams. Denote $\mathcal{S}$ as the set of the satellites and $\mathcal{K}_s$ as the set of the terminals associated to the s-th satellite. Each satellite generates one beam and all the satellites occupy the same frequency band. The gateway delivers data from the core networks to satellites and collects information from terminals, e.g., channel status, traffic

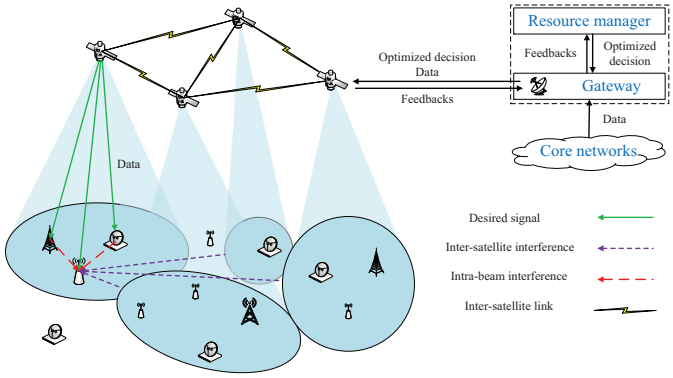

Fig. 2: An illustrative scenario of the considered LEO satellite system. Adaptive beam patterns are adopted to adjust the beam shapes and NOMA is applied in each beam to serve multiple terminals.

demand, terminals' positions, etc. The resource manager, co-located with the gateway, is in charge of executing resource allocation algorithms based on the feedbacks.

Denote $\mathcal{N}_s$ as the set of the candidate beam patterns of satellite s. Each pattern refers to one specific beam shape. With optimized decisions informed by the gateway, one beam pattern is selected out of $\mathcal{N}_s$. Through altering phases and amplitudes by the BFN on the satellite payload, each feed element generates an elementary beam and the shaped beam is constructed by these elementary beams [5]. The resulted beam shape is defined as the coverage within the φ-dB contour, which can be regular (e.g., circular or elliptical beams) or irregular [5].

The relationship between the transmit antenna gain of a beam pattern and the corresponding configuration parameters is sophisticated and may not be captured by explicit expressions, especially for patterns with irregular beam shapes [5], [7], [8]. For better illustration, we use circular beam as an example to abstract the beam pattern model. For the n-th beam pattern of the s-th satellite, the peak gain (regarding the beam center) is expressed as [5], [6],

$$G_{sn,\max}^{\mathrm{tx}} = \frac{\xi\varphi}{3}\left(\frac{70\pi}{\theta_{sn,\varphi\mathrm{dB}}}\right)^2, \tag{1}$$

where ξ is the antenna efficiency and $\theta_{sn,\varphi\mathrm{dB}}$ is the φ-dB angular beamwidth. From (1), we observe that, as the beamwidth increases, the peak gain decreases to disperse outwards to enlarge the coverage. On the other hand, as the beam shrinks, the peak gain increases and the directivity is more concentrated on the beam center. The transmit antenna gain of the s-th satellite to terminal k under the n-th pattern is [5],

$$\left[G_{skn}^{\mathrm{tx}}\right] = \left[G_{sn,\max}^{\mathrm{tx}}\right] - \frac{3G_{sn,\max}^{\mathrm{tx}}}{\xi}\left(\frac{\theta_{sk}}{70\pi}\right)^2, \tag{2}$$

where θ_{sk} is the off-axis angle between the s-th satellite's beam center and the k-th terminal. The operator $[\cdot]$ converts the value into dB. For other types of beam shapes, the expression would be more complicated, e.g., the transmit antenna gain for

elliptical beams depends on beam center position, beamwidth (w.r.t. the major and minor axis), and tilt angle [5], [7].

The channel loss from satellite s to terminal k is,

$$[L_{sk}^{\text{total}}] = [L_{sk}^{\text{ba}}] + [L_{sk}^{\text{ga}}] + [L_{sk}^{\text{sc}}] + [L_{sk}^{\text{ra}}], \tag{3}$$

where L_{sk}^{ga}, L_{sk}^{sc}, and L_{sk}^{ra} are gaseous, scintillation, and rain attenuation exceeded for $\rho\%$ of an average year, respectively. The corresponding models follow 3GPP TR 38.811 [14]. L_{sk}^{ba} is the basic path loss, which is derived by,

$$[L_{sk}^{\text{ba}}] = [L_{sk}] + [L_{sk}^{\text{sf}}], \tag{4}$$

where L_{sk}^{sf} denotes shadow fading following log-normal distribution. L_{sk} denotes the free-space path loss, expressed by,

$$L_{sk} = 32.45 + 20\log_{10}(f^{\text{freq}}) + 20\log_{10}(d_{sk}), \tag{5}$$

where d_{sk} is the distance from satellite s to terminal k, and f^{freq} is the frequency. The channel gain from satellite s to terminal k under beam pattern n is expressed as,

$$|h_{skn}|^2 = G_{skn}^{\text{tx}} G_{sk}^{\text{rx}} / L_{sk}^{\text{total}}. \tag{6}$$

The channel gain from satellite s to terminal k is derived as,

$$|h_{sk}|^2 = \sum_{n\in\mathcal{N}_s} y_{sn}|h_{skn}|^2, \tag{7}$$

where $y_{sn} \in \{0,1\}$ indicates beam pattern selection, where satellite s selects the n-th pattern if $y_{sn}=1$ and not otherwise.

By employing NOMA, each satellite can multiplex at most $\bar{K}$ terminals with different power levels at the same frequency band. We use ϕ_{slk} to indicate the decoding order between terminal k and l served by satellite s. If $\phi_{slk}=0$, terminal k performs SIC to decode l's signal and remove it. If $\phi_{slk}=1$, terminal k views l's signal as noise. Denote p_{sk} as the transmit power of terminal k assigned by satellite s. We apply one of the most widely-adopted rules to decide decoding orders, where the decoding order is identical to the ascending order of $\omega_{sk} = \frac{\sum_{s'\in\mathcal{S}\setminus\{s\}} |h_{s'k}|^2 \sum_{k'\in\mathcal{K}_{s'}} p_{s'k'} + \sigma^2}{|h_{sk}|^2}$ [15], i.e.,

$$\phi_{slk} = \begin{cases} 0, & \text{if } \omega_{sk} \le \omega_{sl}; \\ 1, & \text{otherwise.} \end{cases} \tag{8}$$

The signal-to-interference-plus-noise ratio (SINR) of terminal k associated to satellite s is derived as,

$$\gamma_{sk} = \frac{|h_{sk}|^2 p_{sk}}{I_{sk}^{\text{intra}} + I_{sk}^{\text{inter}} + \sigma^2}, \tag{9}$$

where $I_{sk}^{\text{intra}} = \sum_{l\in\mathcal{K}_s\setminus\{k\}} |h_{sk}|^2 \phi_{slk} p_{sl}$ and $I_{sk}^{\text{inter}} = \sum_{s'\in\mathcal{S}\setminus\{s\}} |h_{s'k}|^2 \sum_{k'\in\mathcal{K}_{s'}} p_{s'k'}$ are intra-beam and inter-satellite interference, respectively. σ^2 is the noise power. The offered capacity of terminal k served by satellite s is,

$$R_{sk} = B\log(1+\gamma_{sk}), \tag{10}$$

where B is bandwidth.

B. Problem Formulation

We formulate a resource allocation problem to jointly optimize power allocation and beam pattern selection to minimize the sum of capacity-demand gap[1]:

$$\mathcal{P}_0: \min_{\mathbf{p},\mathbf{y},\boldsymbol{\phi}} \sum_{s\in\mathcal{S}}\sum_{k\in\mathcal{K}} (R_{sk} - D_{sk})^2 \tag{11a}$$

$$\text{s.t.} \quad \sum_{k\in\mathcal{K}_s} p_{sk} \le \bar{P}_s, \forall s \in \mathcal{S}, \tag{11b}$$

$$\sum_{n\in\mathcal{N}_s} y_{sn} = 1, \forall s \in \mathcal{S}, \tag{11c}$$

$$R_{sk} \ge R_{sk}^{\min}, \forall k \in \mathcal{K}_s \forall s \in \mathcal{S}, \tag{11d}$$

$$\omega_{sk} - \omega_{sl} \le C\phi_{slk}, \forall s \in \mathcal{S}, \forall k, l \in \mathcal{K}_s, k \ne l, \tag{11e}$$

$$\phi_{skl} + \phi_{slk} = 1, \forall s \in \mathcal{S}, \forall k, l \in \mathcal{K}_s, k \ne l, \tag{11f}$$

where $\mathbf{p} \succeq \mathbf{0}$, $\mathbf{y} \in \{0,1\}$, $\boldsymbol{\phi} \in \{0,1\}$ collect all p_{sk}, y_{sn}, and ϕ_{slk}, respectively. In (11b), the total tranmit power of the s-th satellite should be no larger than the power budget $\bar{P}_s$. Constraints (11c) restrict that each satellite can only select one beam pattern. In (11d), terminals' minimum-rate requirements is expressed. Constraints (11e) and (11f) convey the relationship between ω_{sk} and ϕ_{slk} as in (8). Here C is a large number meeting $C \ge \max_{s\in\mathcal{S},k\in\mathcal{K}}\{\omega_{sk}\}$. If $\phi_{slk}=0$, terminal k decodes l's signal and thus $\omega_{sk} \le \omega_{sl}$. If $\phi_{slk}=1$, terminal l decodes k's signal and thus $\omega_{sk} - \omega_{sl} \le C$. Together with constraints (11f) which confine only one decoding order for each satellite beam, we can derive that $\omega_{sk} > \omega_{sl}$.

Due to the non-convexity of the R-function in $\mathbf{p}$, $\mathbf{y}$, and $\boldsymbol{\phi}$ and the presence of binary variables $\mathbf{y}$ and $\boldsymbol{\phi}$, $\mathcal{P}_0$ is identified as mixed-integer nonconvex programming (MINCP) [16]. Thus solving $\mathcal{P}_0$ is a non-trivial task.

III. A Joint Approach for Power Allocation and Beam-Pattern Selection

We provide a joint approach to solve $\mathcal{P}_0$. We first equivalently convert the binary variables into continuous confined by nonlinear equations and then reformulate $\mathcal{P}_0$ into augmented Lagrangian formulation. Next, we design a penalty dual decomposition (PDD) [17] based approach to jointly allocate power and select beam patterns.

We use the following equations to equivalently express $\mathbf{y}$:

$$y_{sn}(1-\bar{y}_{sn}) = 0, \forall s \in \mathcal{S}, \forall n \in \mathcal{N}_s, \tag{12}$$

$$y_{sn} - \bar{y}_{sn} = 0, \forall s \in \mathcal{S}, \forall n \in \mathcal{N}_s, \tag{13}$$

where $\mathbf{y} \in \{0,1\}$ are relaxed into $\mathbf{0} \preceq \mathbf{y} \preceq \mathbf{1}$. $\bar{y}_{sn}$ are auxiliary variables. Equations (12) and (13) are established if and only if $y_{sn} = \bar{y}_{sn} = \{0,1\}$. We use $\bar{\mathbf{y}}$ to collect all $\bar{y}_{sn}$. Since $\boldsymbol{\phi}$ depends on ω_{sk}, we do not directly optimize $\boldsymbol{\phi}$ but decide decoding orders according to (8) when ω_{sk} is updated.

We then rewrite $\mathcal{P}_0$ as the following formulation,

$$\mathcal{P}_0': \min_{\mathbf{p},\mathbf{y},\bar{\mathbf{y}}} \sum_{s\in\mathcal{S}}\sum_{k\in\mathcal{K}_s} (R_{sk} - D_{sk})^2 \tag{14a}$$

[1]Remark that terminal association is assumed given. The optimization problem involving terminal association will be studied in future works.

$$\text{s.t.} \quad (11b), (11c), (11d), (12), (13), \tag{14b}$$

where (12) and (13) are nonlinear equations, leading to the nonconvexity of the problem. Since PDD is designed to tackle the problem with nonlinear equation constraints [17], we propose a PDD-based joint approach. The corresponding augmented Lagrangian function is defined as,

$$\begin{aligned}\mathcal{L}(\mathbf{p},\mathbf{y},\bar{\mathbf{y}};\boldsymbol{\lambda},\boldsymbol{\mu}) = &\sum_{s\in\mathcal{S}}\sum_{k\in\mathcal{K}_s}\left(R_{sk}-D_{sk}\right)^2 \\ &+\frac{1}{2\rho}\left(\sum_{s\in\mathcal{S}}\sum_{n\in\mathcal{N}_s}\left(y_{sn}(1-\bar{y}_{sn})+\rho\lambda_{sn}\right)^2\right. \\ &\left.+\sum_{s\in\mathcal{S}}\sum_{n\in\mathcal{N}_s}\left(y_{sn}-\bar{y}_{sn}+\rho\mu_{sn}\right)^2\right),\end{aligned} \tag{15}$$

where λ_{sn} and μ_{sn} are Lagrangian multipliers for (12) and (13), respectively. $\boldsymbol{\lambda}$ and $\boldsymbol{\mu}$ collect all λ_{sn} and μ_{sn}, respectively. We apply $\rho > 0$ to penalize the objective when the solution does not establish the equations. The augmented Lagrangian problem of $\mathcal{P}_0^{'}$ is expressed as,

$$\mathcal{P}_1: \min_{\mathbf{p},\mathbf{y},\bar{\mathbf{y}}} \mathcal{L}(\mathbf{p},\mathbf{y},\bar{\mathbf{y}};\boldsymbol{\lambda},\boldsymbol{\mu}) \text{ s.t. } (11b), (11c), (11d). \tag{16}$$

The joint approach is executed in a double-loop way. In the inner loop, we decompose $\mathcal{P}_1$ into several solvable subproblems, and then sequentially (or parallely) solve them. In the outer loop, the penalty and Lagrangian multipliers are updated.

A. Inner Loop

At the begining of each iteration, we calculate and sort ω_{sk} to decide decoding orders ϕ_{slk} according to (8). Then we adopt the idea of block coordinate descent (BCD) to decompose $\mathcal{P}_1$ into several subproblems with different blocks of variables.

1) Optimize $\mathbf{p}$*:* We first optimize $\mathbf{p}$ by solving the following subproblem,

$$\min_{\mathbf{p}} \mathcal{F}_1(\mathbf{p}) = \sum_{s\in\mathcal{S}}\sum_{k\in\mathcal{K}_s}\left(R_{sk}-D_{sk}\right)^2 \text{ s.t. } (11b), (11d). \tag{17}$$

We can observe that constraints (11d) are linear as,

$$|h_{sk}|^2 p_{sk} \geq \left(2^{R_{sk}^{\min}}-1\right)\left(I_{sk}^{\text{intra}}+I_{sk}^{\text{inter}}+\sigma^2\right). \tag{18}$$

But $\mathcal{F}_1(\mathbf{p})$ is nonconvex. At the i-th iteration, we approximate $\mathcal{F}_1(\mathbf{p})$ at around $\mathbf{p} = \mathbf{p}^{(i-1)}$ to a surrogate function $\widetilde{\mathcal{F}}_1(\mathbf{p})$, which should satisfy the following two conditions:

- $\widetilde{\mathcal{F}}_1(\mathbf{p})$ is strictly convex in $\mathbf{p}$;
- $\triangledown\widetilde{\mathcal{F}}_1(\mathbf{p}^{(i-1)}) = \triangledown\mathcal{F}_1(\mathbf{p}^{(i-1)})$, where $\triangledown\mathcal{F}_1(\cdot)$ is the gradient.

Based on the conditions, we apply the following surrogate function,

$$\widetilde{\mathcal{F}}_1(\mathbf{p}) = (\mathbf{p}-\mathbf{p}^{(i-1)})\triangledown\mathcal{F}_1(\mathbf{p}^{(i-1)}) + \frac{1}{2\alpha}\|\mathbf{p}-\mathbf{p}^{(i-1)}\|^2, \tag{19}$$

where $\alpha > 0$. The gradient is computed by deriving the partial derivatives as in (20). Then we solve the following problem,

$$\min_{\mathbf{p}} \widetilde{\mathcal{F}}_1(\mathbf{p}) \text{ s.t. } (11b), (11d), \tag{21}$$

which is quadratic convex programming. The optimal solution $\mathbf{p}^*$ can be solved by interior-point method [16]. Then we update $\mathbf{p}$ by the following rule,

$$\mathbf{p}^{(i)} = \mathbf{p}^{(i-1)} + \delta_1^{(i)}(\mathbf{p}^* - \mathbf{p}^{(i-1)}), \tag{22}$$

where $\delta_1^{(i)}$ is the stepsize for updating $\mathbf{p}$ at the i-th iteration.

2) Optimize $\mathbf{y}$*:* Then, we solve the following subproblem to optimize $\mathbf{y}$,

$$\begin{aligned}\min_{\mathbf{y}} \mathcal{F}_2(\mathbf{y}) = &\sum_{s\in\mathcal{S}}\sum_{k\in\mathcal{K}_s}\left(R_{sk}-D_{sk}\right)^2 \\ &+\frac{1}{2\rho}\left(\sum_{s\in\mathcal{S}}\sum_{n\in\mathcal{N}_s}\left(y_{sn}(1-\bar{y}_{sn})+\rho\lambda_{sn}\right)^2\right. \\ &\left.+\sum_{s\in\mathcal{S}}\sum_{n\in\mathcal{N}}\left(y_{sn}-\bar{y}_{sn}+\rho\mu_{sn}\right)^2\right) \text{ s.t. } (11c), (11d),\end{aligned} \tag{23}$$

which is nonconvex due to y_{sn} appearing at both numerator and denominator of the SINR funtion in (9). We adopt the following surrogate function to approximate $\mathcal{F}_2(\mathbf{y})$ at $\mathbf{y} = \mathbf{y}^{(i-1)}$,

$$\widetilde{\mathcal{F}}_2(\mathbf{y}) = (\mathbf{y}-\mathbf{y}^{(i-1)})\triangledown\mathcal{F}_2(\mathbf{y}^{(i-1)}) + \frac{1}{2\beta}||\mathbf{y}-\mathbf{y}^{(i-1)}||^2, \tag{24}$$

where $\triangledown\mathcal{F}_2$ collects the partial derivatives, which is derived in (25). Then the problem is converted into,

$$\min_{\mathbf{y}} \widetilde{\mathcal{F}}_2(\mathbf{y}) \text{ s.t. } (11c), (11d). \tag{26}$$

By obtaining the optimal $\mathbf{y}^*$ via interior-point method, we can update $\mathbf{y}$ by,

$$\mathbf{y}^{(i)} = \mathbf{y}^{(i-1)} + \delta_2^{(i)}(\mathbf{y}^* - \mathbf{y}^{(i-1)}), \tag{27}$$

where $\delta_2^{(i)}$ is the stepsize for updating $\mathbf{y}$ at the i-th iteration.

3) Optimize $\bar{\mathbf{y}}$*:* We optimize $\bar{\mathbf{y}}$ by solving the following subproblem,

$$\min_{\bar{\mathbf{y}}} \sum_{s\in\mathcal{S}}\sum_{n\in\mathcal{N}}(y_{sn}(1-\bar{y}_{sn})+\rho\lambda_{sn})^2 + (y_{sn}-\bar{y}_{sn}+\rho\mu_{sn})^2, \tag{28}$$

which can be decomposed into SN convex subproblems:

$$\min_{\bar{y}_{sn}} (y_{sn}(1-\bar{y}_{sn})+\rho\lambda_{sn})^2 + (y_{sn}-\bar{y}_{sn}+\rho\mu_{sn})^2. \tag{29}$$

By letting the first-order partial derivative equal to zero, the optimal $\bar{y}_{sn}$ can be obtained by,

$$\bar{y}_{sn} = \frac{y_{sn}+y_{sn}^2+\rho\mu_{sn}+\rho\lambda_{sn}y_{sn}}{1+y_{sn}^2}. \tag{30}$$

B. Outer Loop

In the outer loop, we update the Lagrangian multipliers as,

$$\lambda_{sn} = \lambda_{sn} + \frac{1}{\rho}y_{sn}(1-\bar{y}_{sn}), \mu_{sn} = \mu_{sn} + \frac{1}{\rho}(y_{sn}-\bar{y}_{sn}). \tag{31}$$

The the penalty is updated by,

$$\rho = \rho\eta, \tag{32}$$

where $0 < \eta \leq 1$.

$$\begin{aligned}\frac{\partial \mathcal{F}_1}{\partial p_{sk}} =& 2B(R_{sk}-D_{sk})\left(\frac{|h_{sk}|^2}{|h_{sk}|^2 p_{sk}+I_{sk}^{\text{intra}}+I_{sk}^{\text{inter}}+\sigma^2}\right)\\ &+\sum_{l\in\mathcal{K}_s\setminus\{k\}} 2B(R_{sl}-D_{sl})\left(\frac{|h_{sl}|^2\phi_{slk}}{|h_{sl}|^2 p_{sl}+I_{sl}^{\text{intra}}+I_{sl}^{\text{inter}}+\sigma^2}-\frac{|h_{sl}|^2\phi_{slk}}{I_{sl}^{\text{intra}}+I_{sl}^{\text{inter}}+\sigma^2}\right)\\ &+\sum_{s'\in\mathcal{S}\setminus\{s\}}\sum_{k'\in\mathcal{K}_{s'}} 2B(R_{s'k'}-D_{s'k'})\left(\frac{|h_{sk'}|^2}{|h_{s'k'}|^2 p_{s'k'}+I_{s'k'}^{\text{intra}}+I_{s'k'}^{\text{inter}}+\sigma^2}-\frac{|h_{sk'}|^2}{I_{s'k'}^{\text{intra}}+I_{s'k'}^{\text{inter}}+\sigma^2}\right)\end{aligned} \tag{20}$$

$$\begin{aligned}\frac{\partial \mathcal{F}_2}{\partial y_{sn}} =& \sum_{k\in\mathcal{K}_s} 2B(R_{sk}-D_{sk})\left(\frac{|h_{skn}|^2\left(p_{sk}+\sum_{l\in\mathcal{K}_s\setminus\{k\}}\phi_{slk}p_{sl}\right)}{|h_{sk}|^2 p_{sk}+I_{sk}^{\text{intra}}+I_{sk}^{\text{inter}}+\sigma^2}-\frac{|h_{skn}|^2\sum_{l\in\mathcal{K}_s\setminus\{k\}}\phi_{slk}p_{sl}}{I_{sk}^{\text{intra}}+I_{sk}^{\text{inter}}+\sigma^2}\right)\\ &+\sum_{s'\in\mathcal{S}\setminus\{s\}}\sum_{k'\in\mathcal{K}_{s'}} 2B(R_{s'k'}-D_{s'k'})\left(\frac{|h_{sk'n}|^2\sum_{k\in\mathcal{K}_s}p_{sk}}{|h_{s'k'}|^2 p_{s'k'}+I_{s'k'}^{\text{intra}}+I_{s'k'}^{\text{inter}}+\sigma^2}-\frac{|h_{sk'n}|^2\sum_{k\in\mathcal{K}_s}p_{sk}}{I_{s'k'}^{\text{intra}}+I_{s'k'}^{\text{inter}}+\sigma^2}\right)\end{aligned} \tag{25}$$

Algorithm 1 Joint Power Allocation and Pattern Selection

Input: Initialized $\mathbf{p}$, $\mathbf{y}$, $\bar{\mathbf{y}}$.
1: **repeat**
2: **repeat**
3: Calculate ω_{sk} and update $\boldsymbol{\phi}$ by (8).
4: Solve problem (21) and update $\mathbf{p}$ by (22).
5: Solve problem (26) and update $\mathbf{y}$ by (27).
6: Update $\bar{\mathbf{y}}$ by (30).
7: **until** Convergence or reaching I iterations
8: Update $\boldsymbol{\lambda}$ and $\boldsymbol{\mu}$ by (31) and ρ by (32).
9: **until** Convergence or reaching J iterations
Output: Optimized $\mathbf{p}$, $\mathbf{y}$, $\boldsymbol{\phi}$.

The procedure of the joint scheme is summarized in Alg. 1. The inner loop (line 2 to line 8) iterates until it converges or reaches the maximum number of iteration I. The outer loop (line 1 to line 10) terminates when convergence or reaching J iterations. The complexity of Alg. 1 mainly falls into solving convex quadratic programming problems in (21) and (26). Assume $K=\max_{s\in\mathcal{S}}\{K_s\}$ and $N=\max_{s\in\mathcal{S}}\{N_s\}$. The complexity of solving problem (21), which contains SK variables and $S+SK$ linear constraints, is $\mathcal{O}(S^3K^3(S+SK))$ [18]. Similarly, problem (26) is with SN variables and $S+SK$ linear constraints, thus the corresponding complexity is $\mathcal{O}(S^3N^3(S+SK))$. The overall complexity of Alg. 1 is $\mathcal{O}(JIS^3(S+SK)(K^3+N^3))$.

IV. Numerical Results

In simulation, we consider a square area with 500×500 km^2. Denote $\bar{K}$ as the number of multiplexed terminals. Each satellite chooses $\bar{K}$ terminals with the best channel gains. The optimization involving terminal association will be discussed in future works. The parameters are summarized in Table I, unless otherwise stated. We consider beam patterns which generate circular beams with 4.3-dB beamwidths $\{1.2°, 1.8°, 2.4°, 4.8°, 9.6°\}$. Beams with $1.2°$ beamwidth have the largest directivity to the beam center and smallest inter-satellite interference whereas those with $9.6°$ beamwidth generate the widest service range but large interference to terminals associated to adjacent satellites. For pracitcal consideration, we assume the decoding error ratio due to SIC imperfection is 10^{-3}. The results are averaged over 500 instances.

TABLE I: Simulation parameters

Parameter	Value
Frequency, f^{freq}	20 GHz (Ka band)
Bandwidth, W	400 MHz
Satellite height	600 km
Number of satellites, S	5
Power budget, $\bar{P}_s$	43 dBm
Receive antenna gain	42, 36, 32 dBi
Noise power, σ^2	-126.47 dBW
Minimum association rate, $R_k^{\min}$	500 kbps
Number of iteration, I, J	200, 20

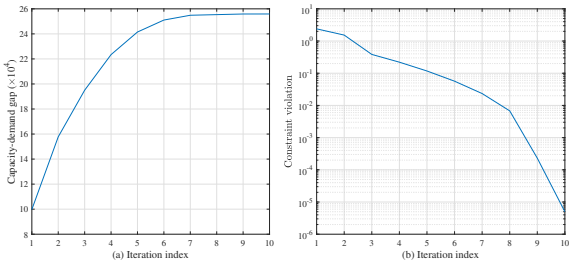

Fig. 3: Convergence performance of Alg. 1: (a) Evolution of capacity-demand gap; (b) Constraint violation.

In Fig. 3, we present the convergence performance of Alg. 1. The capacity-demand gap increases as the algorithm evolves, and eventually converges at the 7-th iteration. At the end of the iterations, the constraint violation maintains at below 10^{-5}, which guarantees the establishment of the equality constraints (12) and (13).

We evaluate the gap performance of the proposed scheme w.r.t. the number of multiplexed terminals $\bar{K}$ in Fig. 4(a). Note that the case of $\bar{K}=1$ refers to the conventional

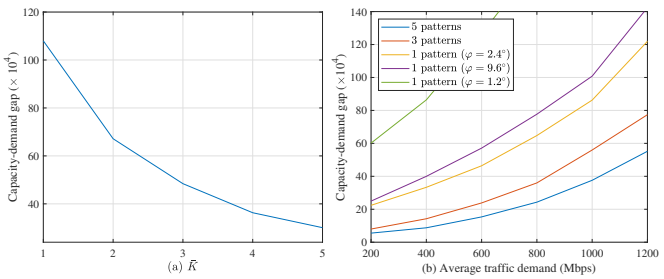

Fig. 4: Gap performance w.r.t. (a) different $\bar{K}$; (b) average traffic demand ($\bar{K} = 3$).

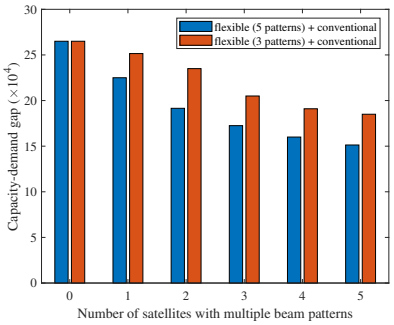

Fig. 5: Performance evaluation in the scenarios with the coexistence of satellites with single pattern (beamwidth $2.4°$) and multiple patterns.

OMA scheme. Compared to the OMA scheme, NOMA has performance gain from 37.8% ($\bar{K} = 2$) to 72.2% ($\bar{K} = 5$) in minimizing the capacity-demand gap. In Fig. 4(b), we compare the performance of the proposed scheme between multiple beam patterns and fixed single beam pattern. Among the three fixed-pattern schemes, the one with $2.4°$ beamwidth outperforms the other two, demonstrating the necessity of appropriate selection of beam patterns. The performance is largely improved by introducing spatial-domain flexibility compared to conventional single beam pattern schemes. Compared to the scheme with fixed $2.4°$ beamwidth, the schemes with 3 patterns and 5 patterns have reduction of 42.5% and 60.9% in capacity-demand gap.

In practice, LEO satellites functioned with adaptive beam patterns would coexist with those with conventional payloads in the system. We evaluate the scenarios with the coexistence of different types of LEO satellites in Fig. 5. By introducing satellites with adaptive beam patterns, the capacity-demand gap can be largely reduced, from 26.5×10^4 to 15.1×10^4 and 18.5×10^4 when introducing 5 and 3 beam patterns, respectively. The more satellites with spatial-domain flexibility, the more performance gain is obtained.

V. Conclusion

In this paper, we have investigated potential synergies of adaptive beam patterns and NOMA in a LEO satellite system. We have formulated an resource problem of jointly optimizing power allocation and beam pattern selection. We have discussed how to tackle nonconvexity and binary variables and designed a joint scheme to solve the problem. Finally we have evaluated the performance and demonstrated the superiority of the joint scheme over benchmarks.

Acknowledgement

This work has been supported by the Luxembourg national research fund (FNR) under the project ROSETTA (C17/IS/11632107) and MegaLEO (C20/IS/14767486).

References

[1] H. Al-Hraishawi, H. Chougrani, S. Kisseleff, E. Lagunas, and S. Chatzinotas, "A survey on non-geostationary satellite systems: The communication perspective," *arXiv preprint arXiv:2107.05312*, 2021.

[2] S. Xia, Q. Jiang, C. Zou, and G. Li, "Beam coverage comparison of LEO satellite systems based on user diversification," *IEEE access*, vol. 7, pp. 181 656–181 667, 2019.

[3] M. Y. Abdelsadek, H. Yanikomeroglu, and G. K. Kurt, "Future ultra-dense LEO satellite networks: A cell-free massive MIMO approach," in *2021 IEEE International Conference on Communications Workshops (ICC Workshops)*. IEEE, 2021, pp. 1–6.

[4] S. Kisseleff, E. Lagunas, T. S. Abdu, S. Chatzinotas, and B. Ottersten, "Radio resource management techniques for multibeam satellite systems," *IEEE Communications Letters*, vol. 25, no. 8, pp. 2448–2452, 2020.

[5] G. Maral, M. Bousquet, and Z. Sun, *Satellite communications systems: Systems, techniques and technology*. John Wiley & Sons, 2020.

[6] M. Takahashi, Y. Kawamoto, N. Kato, A. Miura, and M. Toyoshima, "Adaptive power resource allocation with multi-beam directivity control in high-throughput satellite communication systems," *IEEE Wireless Communications Letters*, vol. 8, no. 4, pp. 1248–1251, 2019.

[7] P. J. Honnaiah, N. Maturo, S. Chatzinotas, S. Kisseleff, and J. Krause, "Demand-based adaptive multi-beam pattern and footprint planning for high throughput GEO satellite systems," *IEEE Open Journal of the Communications Society*, vol. 2, pp. 1526–1540, 2021.

[8] F. G. Ortiz-Gomez, M. A. Salas-Natera, R. Martínez, and S. Landeros-Ayala, "Optimization in VHTS satellite system design with irregular beam coverage for non-uniform traffic distribution," *Remote Sensing*, vol. 13, no. 13, p. 2642, 2021.

[9] S. Tani, K. Motoyoshi, H. Sano, A. Okamura, H. Nishiyama, and N. Kato, "An adaptive beam control technique for Q band satellite to maximize diversity gain and mitigate interference to terrestrial networks," *IEEE Transactions on Emerging Topics in Computing*, vol. 7, no. 1, pp. 115–122, 2016.

[10] A. Guidotti, "Beam size design for new radio satellite communications systems," *IEEE Transactions on Vehicular Technology*, vol. 68, no. 11, pp. 11 379–11 383, 2019.

[11] X. Yan, K. An, T. Liang, G. Zheng, Z. Ding, S. Chatzinotas, and Y. Liu, "The application of power-domain non-orthogonal multiple access in satellite communication networks," *IEEE Access*, vol. 7, pp. 63 531–63 539, 2019.

[12] J. Chu, X. Chen, C. Zhong, and Z. Zhang, "Robust design for NOMA-based multibeam LEO satellite internet of things," *IEEE Internet of Things journal*, vol. 8, no. 3, pp. 1959–1970, 2020.

[13] Z. Gao, A. Liu, C. Han, and X. Liang, "Files delivery and share optimization in LEO satellite-terrestrial integrated networks: A NOMA based coalition formation game approach," *IEEE Transactions on Vehicular Technology*, 2021.

[14] 3GPP TR 38.811, "Technical specification group radio access network; Study on new radio (NR) to support non-terrestrial networks (Release 15), v15.4.0," 2020.

[15] A. Wang, L. Lei, E. Lagunas, A. I. Pérez-Neira, S. Chatzinotas, and B. Ottersten, "NOMA-enabled multi-beam satellite systems: Joint optimization to overcome offered-requested data mismatches," *IEEE Transactions on Vehicular Technology*, vol. 70, no. 1, pp. 900–913, 2020.

[16] S. Boyd and L. Vandenberghe, *Convex optimization*. Cambridge university press, 2004.

[17] Q. Shi and M. Hong, "Penalty dual decomposition method for non-smooth nonconvex optimization—part I: Algorithms and convergence analysis," *IEEE Transactions on Signal Processing*, vol. 68, pp. 4108–4122, 2020.

[18] P. Gahinet, A. Nemirovski, A. J. Laub, and M. Chilali, *LMI Control Toolbox Users Guide*. MathWorks, 1995.